Hydrogen Bonding of Water Confined in Mesoporous Silica MCM-41 and SBA-15 Studied by ^{1}H Solid-State NMR

Bob Grünberg,[a] Thomas Emmler,[a] Egbert Gedat,[a] Ilja Shenderovich,[a] Gerhard H. Findenegg,[b] Hans-Heinrich Limbach,*[a] and Gerd Buntkowsky*[a]

Abstract: The adsorption of water in two mesoporous silica materials with cylindrical pores of uniform diameter, MCM-41 and SBA-15, was studied by ^{1}H MAS (MAS = magic angle spinning) and static solid-state NMR spectroscopy. All observed hydrogen atoms are either surface −SiOH groups or hydrogen-bonded water molecules. Unlike MCM-41, some strongly bound water molecules exist at the inner surfaces of SBA-15 that are assigned to surface defects. At higher filling levels, a further difference between MCM-41 and SBA-15 is observed. Water molecules in MCM-41 exhibit a bimodal line distribution of chemical shifts, with one peak at the position of inner-bulk water, and the second peak at the position of water molecules in fast exchange with surface −SiOH groups. In SBA-15, a single line is observed that shifts continuously as the pore filling is increased. This result is attributed to a different pore-filling mechanism for the two silica materials. In MCM-41, due to its small pore diameter (3.3 nm), pore filling by pore condensation (*axial*-pore-filling mode) occurs at a low relative pressure, corresponding roughly to a single adsorbed monolayer. For SBA-15, owing to its larger pore diameter (8 nm), a gradual increase in the thickness of the adsorbed layer (*radial*-pore-filling mode) prevails until pore condensation takes place at a higher level of pore filling.

Keywords: monolayers · NMR spectroscopy · pore condensation · water chemistry · zeolite analogues

Introduction

Water is the primary solvent for most naturally occurring chemical and biological reactions. The special physical properties of water stem largely from its extraordinary internal cohesiveness, compared with most other liquids of similar molecular weights. This cohesiveness is mainly the result of water molecules' high polarity and their ability to form hydrogen-bonded networks among themselves, as for example, in the frozen phase or in the bulk-liquid phase. In restricted geometries, water molecules can also interact with surfaces through hydrophobic and hydrophilic interactions and hydrogen-bond interactions; hence there is competition between the surface–liquid and liquid–liquid interactions. This competition can lead to interesting new structures of the water that are not observed in bulk water. In particular, at least partial ordering of the water molecules in the vicinity of the confining surface is often found. Important examples of such systems are water molecules enclosed in porous media like zeolites[1] or cements,[2] or water molecules in hydration shells of proteins.[3–8] Specifically, the existence of two kinds of water in pores, free water in the center of the pore and bound water near the pore surface, has been established by a variety of experimental techniques.[1, 9–19] Analyzing these structures may help in the understanding of the water–surface interaction at the molecular level. For this analysis a molecular observable must be studied, which is sensitive to the structure and binding of individual water molecules. The ^{1}H chemical shift of water molecules is such an observable. Its value depends strongly on the structural and dynamical properties of the hydrogen atoms. Because the observed phases are often ordered, that is, anisotropic, one can also expect at least some residual anisotropy in the NMR parameters of the system. Therefore, these systems have to be studied employing ^{1}H solid-state NMR spectroscopy.

In the present work, we study water as a guest molecule in mesoporous silica of MCM-41[20] and SBA-15[21] types. These materials constitute two-dimensionally hexagonal arrays of cylindrical pores of uniform size in the range between 2–10 nm.[22] Due to this wide range of available pore

[a] B. Grünberg, T. Emmler, Dr. E. Gedat, Dr. I. Shenderovich, Prof. Dr. H.-H. Limbach, Priv. Doz. Dr. G. Buntkowsky
Freie Universität Berlin, Institut für Chemie
Takustrasse 3, 14195 Berlin (Germany)
Fax: (+49) 30-838-55310
E-mail: limbach@chemie.fu-berlin.de
    bunt@chemie.fu-berlin.de

[b] Prof. Dr. G. H. Findenegg
Technische Universität Berlin
Stranski Laboratorium für Physikalische und Theoretische Chemie
Strasse des 17. Juni 112, 10623 Berlin (Germany)

sizes, they are very versatile molecular sieves. Whereas MCM-41 silicas have pore sizes in the range of 2–6 nm and smooth pore surfaces, SBA-15 silicas can be typically prepared in the range of 5–10 nm and exhibit considerable surface roughness, which is attributed to $(SiO_2)_n$ islands on the surface.[23] Owing to the high density of pores and the relatively small pore diameters, these silica materials have extremely large inner surfaces, relative to the volume of the individual particle. The particle size is typically in the range of 5 μm. The pore-to-pore distance, which is estimated as the inverse length of the scattering vector in X-ray diffraction, is about 20% larger than the pore diameter. The geometry of the pores is highly anisotropic, such that a preferred axis exists in the direction of the pores' cylinder axis, and diffusion of guest molecules in the pores is found to exhibit deviations from ordinary diffusion.[24] Moreover, these surface effects influence not only the translational, but also the rotational degrees of freedom of guest molecules, as was shown recently by low-temperature ^2H NMR spectroscopy.[25] Since the physical properties of their inner surfaces, such as the surface acidity, can be chemically modified,[26,27] mesoporous silica materials are very promising candidates for catalytic applications; this interest has triggered several recent studies of the dynamics of guest molecules in mesoporous silica.[28–34]

Experimental Section

Preparation of mesoporous silica MCM-41: The MCM-41 material was synthesized according to the method of Grün et al.[35] using cetyltrimethylammonium bromide ($C_{16}TAB$) as the template. $C_{16}TAB$ (2.36 g) dissolved in water (120 g) was mixed with aqueous ammonia (9.5 g, 25 wt%). Then tetraethoxysilane (TEOS, 10 g) was added under constant stirring at 35°C. The precipitated product was kept in the reaction solution at 80°C for 72 h and then filtered and washed with deionized water. After drying in air at 105°C for 5 h, the product was heated to 550°C (1 K min^{-1}) and calcined under flowing air. The mesoscopic structure and the porosity of the MCM-41 material were characterized by X-ray diffraction and gas adsorption as explained elsewhere.[36] The X-ray diffraction pattern of the calcined MCM-41 sample exhibited four well-resolved peaks conforming to a two-dimensional hexagonal lattice (space group $p6mm$) with a lattice spacing of $d_{100} = 4.0$ nm (pore-to-pore distance $a_0 = 4.6$ nm). The nitrogen adsorption isotherm at 77 K (Figure 1a)

was measured by gas volumetry using a Gemini 2375 apparatus (Micromeritics). The BET surface area (S) was measured as 1040 m^{2}g^{-1} and the specific pore volume (V) as 0.93 cm^{3}g^{-1}. The pore diameter of $d = 3.3$ nm was calculated by the method of Dollimore and Heal.[37]

Preparation of mesoporous silica SBA-15: The silica was prepared according to the method of Zhao et al.[21] employing Pluronic P103 [EO$_{17}$–PO$_{55}$–EO$_{17}$, EO = poly(ethylene oxide), PO = poly(propylene oxide); BASF, Mt. Olive, NJ, USA] as the templating agent. P103 (8 g) was dissolved in distilled water (480 mL) and 97% H_2SO_4 (26 mL) was added to the solution. Then TEOS (18.4 mL) was added under stirring at a temperature of 40°C. The solution was first kept at 40°C for 5 h and then at 108°C for another 24 h. The product was rinsed with deionized water and calcined at 550°C. Two different batches of SBA-15 were used (TLX-1 and PLX-A). The X-ray measurement indicated that the silica was ordered in a two-dimensional hexagonal lattice with a lattice constant of $d_{100} = 8.7$ nm (pore-to-pore distance $a_0 = 10.0$ nm). The pore diameters of 8.0 nm (TLX-1) and 7.9 nm (PLX-A) were determined from the adsorption branch of the nitrogen isotherm (Figure 1b) employing the Dollimore—Heal formalism.[37] The BET surface area (S) and the specific pore volume (V), as determined from the N$_2$ gas adsorption isotherm, were 720 m^{2}g^{-1} and 0.96 cm^{3}g^{-1}, respectively, for TLX-1, and 791 m^{2}g^{-1} and 1.01 cm^{3}g^{-1}, respectively, for PLX-A.

^1H solid-state NMR spectroscopy: All ^1H NMR measurements were performed on a Bruker MSL-300 instrument, operating at 7 T, equipped with a Bruker 4 mm single resonance ^1H CRAMPS probe. The room temperature static and magic angle spinning (10000 Hz) NMR experiments were performed by employing a π/2 pulse sequence with full CYCLOPS phase cycling. The 90°-pulse length was 3.2 μs for ^1H and the sweep width was 10 kHz. All chemical shift values are referenced to tetramethylsilane (TMS), with water as an external standard.

NMR samples: To obtain reproducible results the silica–water samples were prepared in the following way. The dried silica was weighted and filled into a 4 mm rotor (MCM-41: 14.99 ± 0.05 mg; SBA-15: 19.76 ± 0.05 mg). To remove physisorbed and hydrogen-bonded water without causing dehydroxylation of silanol groups, the samples were dried under high vacuum (ca. 10^{-6} mbar) for 24 h at a moderate temperature of 400 K. Then a defined amount of water was added by means of a calibrated micropipette. The absolute amount of water was determined using a microbalance (Sartorius) with an accuracy of ± 0.05 mg. Employing this value and the known surface area of the silica, we determined the coverage of the surfaces. The spectra at the various water contents were obtained as follows: The rotor was closed with the rotor cap, which sealed the rotor sufficiently to prevent evaporation of the water during the ^1H NMR measurements, and the sample was weighted and measured. After measurement, the rotor was opened again and part of the water was removed by heating the rotor with a heat gun. The rotor was closed again with the cap, weighted and measured. Precise data of the samples are given in Tables 1 and 2.
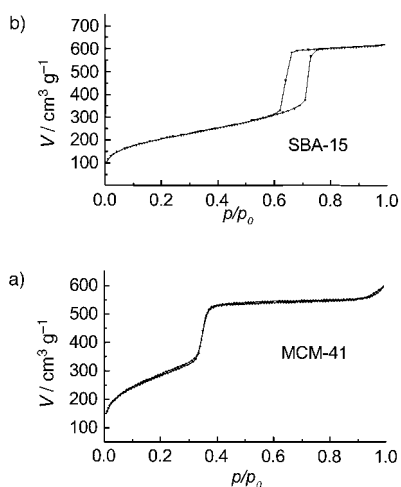

Figure 1. Nitrogen isotherms of a) MCM-41 and b) SBA-15.

Table 1. Water content of the MCM samples.

Sample[a]	n [(H_2O) per nm^2][b]	Vol%[c]	m [mg][d]
a	30.8	100	14.33
b	6.8	23	3.19
c	1.7	6	0.80
d	0.94	3.2	0.44
e	0.8	2.7	0.37
f	< 0.05	< 0.05	0

[a] The identifier for each sample (see the spectra in Figure 2). [b] The number of H_2O molecules on the surface per nm^2 (calculated with respect to the specific surface area, S). [c] The content of H_2O in Vol% (calculated with respect to the specific pore volume, V). [d] The mass of water for each sample (measured with a precision microscale from Sartorius).

Table 2. Water content of the SBA samples.

Sample[a]	n [(H_2O) per nm^2][b]	Vol %[c]	m [mg][d]
a[e]	38.2	96.0	14.36
b[e]	17.4	43.8	6.56
c[e]	8.0	20.0	3.01
d	3.6	8.1	1.53
e	1.4	3.2	0.60
f	0.4	1.0	0.18
g	0.3	0.7	0.13
h	0.24	0.5	0.10
i	<0.1	<0.1	<0.02
j	<0.05	<0.05	0

[a] The identifier for each sample (see the spectra in Figure 3). [b] The number of H_2O molecules on the surface per nm^2 (calculated with respect to the specific surface area, S). [c] The content of H_2O in Vol% (calculated with respect to the specific pore volume, V). [d] The mass of water for each sample (measured with a precision microbalance from Sartorius). [e] The samples a, b and c consist of SBA-15 batch PLX-A instead of SBA-15 batch TLX-1.

Results

Before discussing the individual spectra, we wish to report that the filling and emptying of the pores with water was completely reversible. By employing a heat gun with moderate heating (see SBA-15 below), it was possible to completely empty the pores after filling them with a definite amount of water. Thus in principle, the filling and emptying cycle can be repeated as often as desired.

^{1}H NMR of water in MCM-41: Figure 2 displays the rotating and nonrotating ^{1}H NMR spectra of water in MCM-41 for different water contents. While the ^{1}H MAS spectra (left) in general exhibit several resolved lines with typical line widths of 0.3–0.6 ppm, in the static spectra (right) only relatively

broad lines are visible and individual sites are only reflected by shoulders in the line shape. The MAS spectrum that was measured after drying the sample on the vacuum line (spectrum f) exhibits only a single line at $\delta = 1.74$ ppm, which we label as **I**. Figure 2e displays the spectrum with the lowest water content of 2.7%. Here the spectrum is still dominated by signal **I**, but a slight increase in the line width is observed. Additional spectral intensity is visible as a high field socket of the line (**II**) and as a weak signal (**III**) appearing at about 2.5 ppm. Upon further increase of the water content to 3.2% (Figure 2d), the 1.74 ppm line continues to increase in width, and the line at 2.5 ppm grows strongly and finally starts to dominate the spectrum in the sample with 6% (c). Upon further increase of the water content to 23% (b) this line is broadened and low-field shifted to 3.4 ppm. In addition, a new signal appears at 4.7 ppm (**IVa**) that finally, in the completely filled sample with 100% water content (a), is the only visible line in the spectrum. In addition to these relatively narrow lines, a weak, broad background signal, which covers the whole range from 1 to 6 ppm, is visible in spectra (c) and (d).

Comparing these MAS results with the static spectra, several striking differences are evident: Firstly, the width of the line (Figure 2 right panel) is significantly larger than the width of the MAS lines. As a result of this, the individual lines visible in the MAS spectra are only indicated by the shoulders in the line shape. Secondly, in the spectra with very low water contents (spectra e and f) no signal is visible at all. In the spectra with intermediate water contents (c and d) only a broad signal between 2 ppm and 3 ppm is visible, and in the samples with high water contents (a and b) a very broad asymmetric signal at 4.70 ppm is visible. For the analysis of signals in spectra a and b, a deconvolution of the line shape into two individual lines was performed, employing the values of the isotropic shift from the MAS experiments.
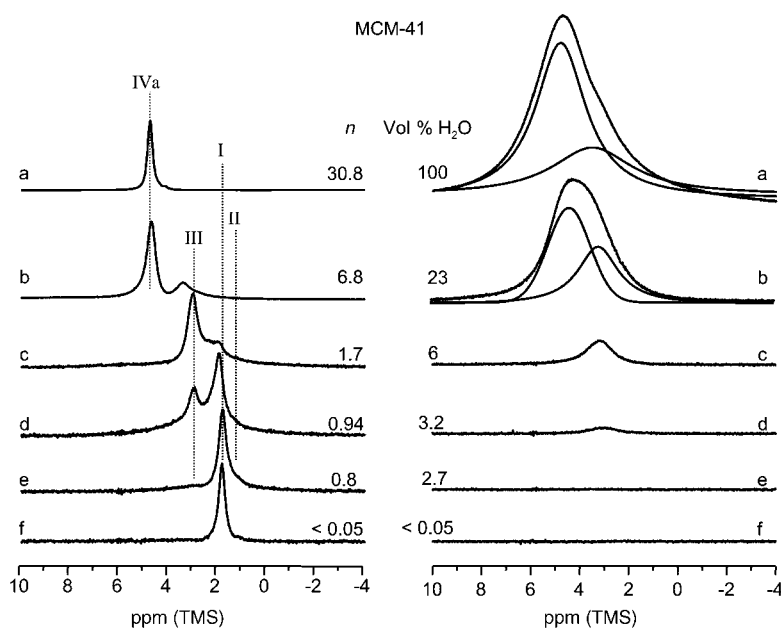
^{1}H NMR of water in SBA-15: Owing to the larger pore diameter with the correspondingly lower relative surface, lower water fillings were employed for the SBA-15 sample. Figure 3 displays the rotating (left) and nonrotating (right) ^{1}H NMR spectra of water in SBA-15 for different water contents. Again in the ^{1}H MAS spectra in general several resolved lines are visible. The typical line widths of 0.2–0.4 ppm are more narrow than the corresponding line widths in the MCM-41 samples. The MAS spectra of the samples with the low water contents (Figure 3h–j) exhibit the same line **I** at $\delta = 1.74$ ppm that is observed in the MCM-41 samples. However,
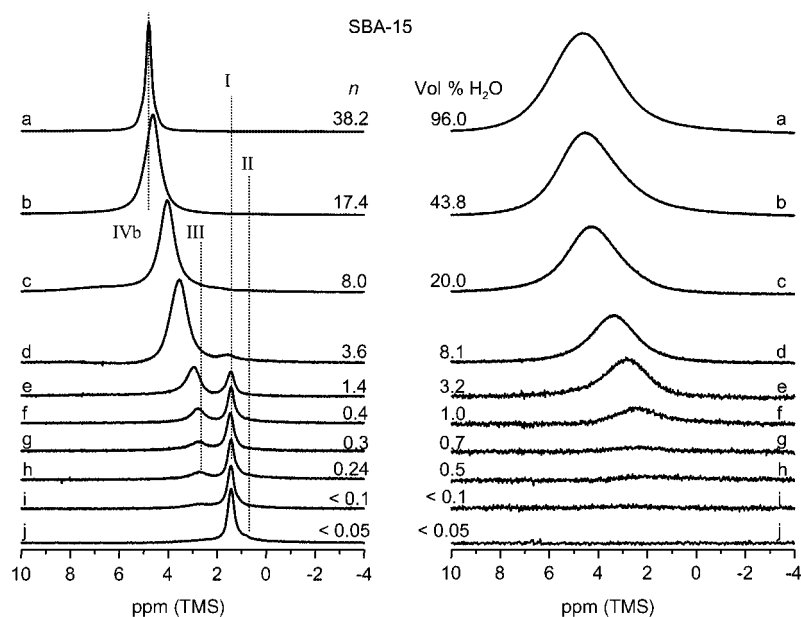

Figure 2. Experimental ^{1}H solid-state NMR spectra of water in MCM-41 at varying water contents ($n =$ number of H_2O molecules on the surface per nm^2). The letters correspond to those in Table 1. Right panel: static (nonrotating) spectra. Left panel: MAS spectra normalized to the same maximum height.

Figure 3. Experimental ^{1}H solid-state NMR spectra of water in SBA-15 at varying water contents (n = number of H_2O molecules on the surface per nm^2). The letters correspond to those in Table 2. Right panel: static (non-rotating) spectra. Left panel: MAS spectra, normalized to the same maximum height.

by an individual ^{1}H chemical shift. While in principle these ^{1}H chemical shifts are unique for a defined structure of the water molecule interacting with the surface and other water molecules, in practice it must be taken into account that dynamic exchange effects, like molecular rotations of the water molecules, rotations of the surface −SiOH groups, and proton transfer, can, and in general will, cause exchange between these different chemical shifts; this effect leads to complete or full averaging of the line positions.

Nevertheless, it is still possible to distinguish between different environments, and thus determine the relative amounts of the individual species, which is done in the following way. As
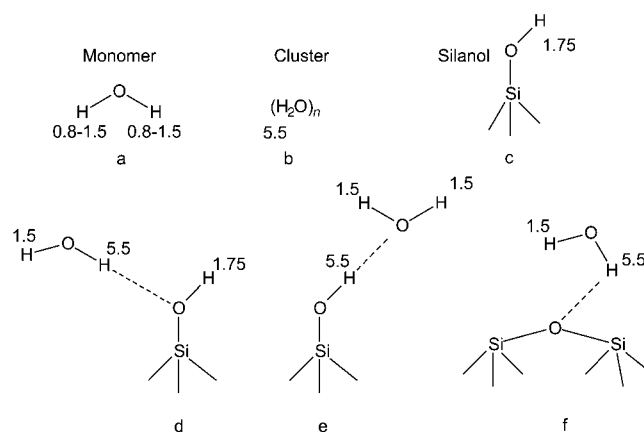
even in the nominally completely dried sample (i) there is some spectral intensity between 2 and 3 ppm. To remove this water, an additional drying of the sample for 48 h at 120 °C on the vacuum line was necessary. This drying removed the remaining water visible in spectrum i. Upon increase of the water content to 0.5 %, again a slight increase of the line width is observed, accompanied by the growth of line **III** at 2.5 ppm. Again, the position of this line shifts slightly to low-field upon increase of the water content to 3.2 % (e), and the width of the line increases. At 8 % filling (d) the line at 1.74 ppm is only barely visible, and the spectrum is dominated by a broad line at 3.9 ppm. Further increase of the water content (a–c) shifts this line smoothly to the final value of 5 ppm (**IVb**). Again, in addition to these relatively narrow lines, a weak, broad background signal that covers the whole range from 1 to 6 ppm is visible in spectrum c.

In the static spectra, no signal is visible in the samples with fillings below 0.7 %. Above this filling, a relatively broad symmetric line is visible in the spectrum. The position of this line shifts parallel to the MAS signal towards lower fields upon increase of the water content.

Discussion

From the NMR spectra shown above it is evident that different water environments exist inside the mesopores of the silica. These environments can be characterized by their individual chemical shifts. The experimental results are now discussed with respect to the water structures inside the mesopores. Figure 4 displays the different possible scenarios of water molecules hydrogen bonded to the silica surface, or amongst each other, or free. Each scenario is characterized

Figure 4. Overview of possible −OH groups in the water/silica samples and the corresponding chemical shifts in ppm (TMS). Upper row: chemical shifts of the constituents of monomeric water, water clusters and silanol groups. Lower row: chemical shifts observed in various hydrogen-bonding scenarios.

a starting point we want to note that a line between 0.8 and 1.5 ppm is not observed in any spectrum; this line would correspond to protons of monomeric water molecules, that is, protons that do not exhibit any kind of OHO hydrogen bonding. This shows that all water molecules are in a hydrogen-bonded state. Thus, they must either form water clusters or hydrogen bonds with −OH groups on the surface.

By employing this chemical shift information, the results of water in MCM-41 are discussed. In the dried sample (Figure 2f), only a single resonance at δ = 1.74 ppm is observed. Comparing this value to the chemical shift of −SiOH protons in MCM-41[26] (δ = 1.75 ppm), this signal can be attributed to the surface −SiOH protons. This shows that by drying on the vacuum line all water molecules are removed

from MCM-41. From this we can conclude that there is no strongly bound water, for example, due to structural inhomogeneities, or water molecules confined in inaccessible places.

It is interesting to compare this result to the SBA-15 mesopores (Figure 3a–j). Here the simple drying procedure employing the heat gun did not cause a complete removal of all water from the pore (spectrum i). As discussed above, the last water molecules were only removable by drying the sample on the vacuum line at 120 °C (spectrum j). Thus, in contrast to the MCM-41 sample, the SBA-15 sample must possess some kind of structural inhomogeneities that cause a stronger binding or trapping of the water molecules. This observation corroborates results on the roughness of the surface structures of SBA-15 and MCM-41, which were obtained by employing the absorption of ^{15}N and para-^{2}H-labeled pyridine on the surfaces of these pores.[23] It was reported that a fast rotational diffusion combined with a surface-hopping of pyridine molecules on the surfaces of the pores was observed. These combined motions cause a motional averaging of the ^{15}N CSA (CSA = cross-sectional surface area) and ^{2}H quadrupolar tensors of the molecule. While for SBA-15 a complete averaging to an isotropic line was observed, a residual anisotropy remained in MCM-41. The full averaging observed in SBA-15 is only possible in the case of a surface with considerable roughness due to the presence of structural defects. Since the general chemical and crystalline structures of MCM-41 and SBA-15 are very similar with respect to the hydrogen bonding of the water molecules to the surface, these structural defects are the main difference between MCM-41 and SBA-15. Thus, one can conclude that they are responsible for the trapping of the strongly bound water molecules on the surfaces.

Comparing the chemical shifts of the water signals at low filling levels (2.5–3 ppm) with the values given for the possible chemical shifts of −OH groups, it is evident that none of these shifts matches the observed shift. From this it follows that the observed shift is the result of the weighted averaging between different water species, caused by fast chemical exchange among them. This interpretation is supported by the absence of monomeric water units. From Figure 4 it can be seen that the chemical shift of non-hydrogen-bonded water protons is 1.5 ppm. For low water concentrations, where the number of water molecules is below the number of surface −SiOH groups, a static configuration of water molecules in configurations **d** or **e** (see Figure 4) would give rise to such a line. Since this line is not observed one can conclude that all water molecules contribute to hydrogen bonds. The average distance between surface −OH groups can be estimated from their surface densities[23] of $n_{OH} \approx$ 3 nm^{-2} for MCM-41 and $\approx$3.7 nm^{-2} for SBA-15, as 0.58 and 0.52 nm, respectively. These average distances are too large to be bridged by a single hydrogen-bonded water molecule. In other words, only one of the two water protons can be in a hydrogen bond in a given moment. Since both protons are found to be magnetically equivalent, it follows that they are in fast exchange. The assumption of a fast exchange of only the two water protons and a fixed −SiOH···OH$_2$ hydrogen bond would give a line of the water protons at (1.5 + 5.5)/

2 = 3.5 ppm. As the observed line of the water proton is below 3 ppm for low filling factors, one can conclude that a more complicated exchange process, which involves the proton of the −SiOH group, occurs. The simplest mechanism is the mutual exchange of the two water protons with the −SiOH proton.

Assuming a symmetric exchange between all three positions, such an exchange process would cause an average line at (1.5 + 1.75 + 5.5)/3 = 2.9 ppm for configuration **d** and (1.5 + 1.5 + 5.5)/3 = 2.8 ppm for configuration **e** (see Figure 4); these values are closer to those experimentally observed. In practice, one can assume that this process is not a simple chemical exchange of the three protons, but a surface-hopping of the water molecule that is accompanied by the formation and breaking of covalent −OH bonds and O···H hydrogen bonds.

Upon further increase of the water content, two processes start: on the one hand the average of the line is low-field shifted towards the chemical shift values of water clusters, and on the other hand the number of free surface −SiOH groups is reduced, which is visible as a decline in the intensity of the 1.75 ppm line. At a water content of 8 %, which corresponds to about 3.5 water molecules per square nm, the line of the surface −SiOH groups in SBA-15 has practically disappeared. This shows that all −SiOH groups are now part of a hydrogen bond, that is, a network of exchanging hydrogen-bonded protons (see Figure 5). This interpretation is corroborated by the surface density of −SiOH groups, which is $\approx$3.7 nm^{-2} for SBA-15.[23] Upon further increase of the water content, this network of hydrogen-bonded −OH groups is shifted towards lower field, caused by the higher mole fraction of water molecules. Finally, the broad component visible in the MAS spectra of both samples can be attributed to both water domains on the surface, where residual dipolar interactions among the protons are too strong to be fully removed by MAS, and to line broadening caused by chemical exchange.
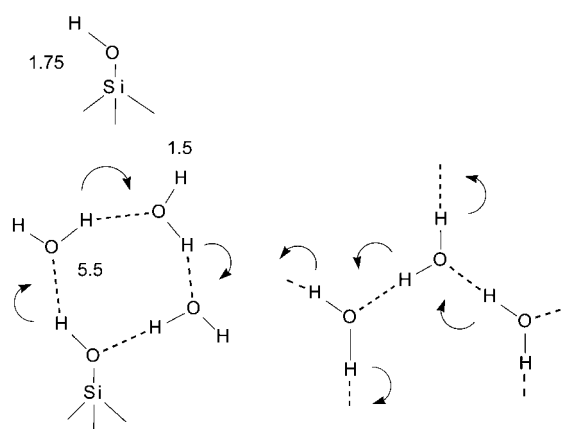

Figure 5. Sketch of possible water configurations hydrogen bonded to the surface −SiOH group and the mutual proton exchange processes in these configurations. The numbers denote the chemical shift typically associated with these configurations.

At intermediate water contents an interesting difference between MCM-41 and SBA-15 is observed. For MCM-41 two separate lines are visible, for example, in the spectrum with 23% water content corresponding to seven water molecules per square nm. The first of these lines is the above discussed line caused by the exchange of water and silica −OH groups. The second, lower field line has a chemical shift of 4.8 ppm. This value lies between the value for free water clusters (5.5 ppm) and the value of the first line. This finding can be interpreted as a bimodal distribution of the thickness of the water layer on the surface, due to the coexistence of filled pores and pores in which only the surface is covered with water. For SBA-15, however, a smooth, low-field shift of the line as a function of the water content is observed; this shift indicates a monomodal distribution of the thickness of the water layer on the surface.
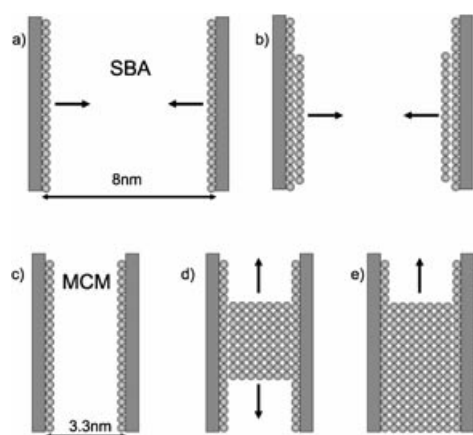

Figure 6. Sketch of the proposed pore-filling mechanisms of SBA-15 (upper row) and MCM-41 (lower row). In SBA-15, with its wider pore diameter, after initial coverage of the surface, a radial growth towards the pore axis is proposed. In MCM-41, however, an axial filling of the pores is proposed.

This finding has important consequences for the filling mechanisms of the pores, which are sketched in Figure 6. In SBA with its large pore diameter of 8 nm, after the initial wetting of the surface (Figure 6a), further filling occurs smoothly from the pore wall towards the center of the pore (Figure 6b), until finally, complete filling of the pores is achieved. In MCM, however, after the initial wetting of the pore surfaces (Figure 6c), a coexistence of filled pores or pore segments with wetted pores or pore segments exists (Figure 6d). Further filling of the pores occurs as a growth of the filled pores (Figure 6e), until again complete filling is achieved. Thus, for SBA the water layer in the pore grows radially towards the pore center, while for MCM the water layer grows axially in the direction of the pore axis.

Finally, for completely filled pores two different chemical shift values are found, namely 4.7 ppm for MCM-41 and 5.0 ppm for SBA-15. These differences are an indication of the different ratio of surface-water molecules to inner-water molecules. Assuming ideally cylindrical pores for simplicity,

the amount of water molecules in a monomolecular water layer on the surface is given by Equation (1) (r_p: pore radius, r_w: radius of a water molecule, ρ_w: density of water).

$$N_S = \rho_w \pi (r_p^2 - (r_p - 2r_w)^2) \tag{1}$$

The number of "inner" water molecules is given in Equation (2).

$$N_I = \rho_w \pi (r_p - 2r_w)^2 \tag{2}$$

The average chemical shift is given in Equation (3).

$$\bar{\delta} = \frac{N_I}{N_I + N_S}\delta_I + \frac{N_S}{N_I + N_S}\delta_S =$$
$$\frac{(r_p - 2r_w)^2}{(r_p - 2r_w)^2 + [r_p^2 - (r_p - 2r_w)^2]}\delta_I + \frac{[r_p^2 - (r_p - 2r_w)^2]}{(r_p - 2r_w)^2 + [r_p^2 - (r_p - 2r_w)^2]}\delta_S \tag{3}$$

For a simple estimation, the radius of a water molecule is estimated from its density as 0.19 nm. By employing this value and the respective pore radii of 1.65 and 4.0 nm, the calculated average chemical shift values are 4.7 ppm for MCM-41 and 5.2 ppm for SBA-15. These values are in very good agreement with the experimentally observed chemical shift values of 4.7 and 5.0 ppm, respectively, particularly when the crudity of the model is taken into account. The greater deviation for SBA-15 might be a result of its higher surface roughness, which makes the pore radius less well defined.

Comparing the static spectra of the empty pores at low water contents for MCM-41 and SBA-15 (right panels of Figures 2 and 3, respectively), it is evident that the line at 1.75 ppm that was visible in the MAS spectra is not visible in the static spectra. This result corroborates our interpretation that this line has to be attributed to immobile surface −SiOH groups. From their average distance on the surface, a mutual ^{1}H–^{1}H dipolar coupling constant of 4 kHz can be calculated; this coupling causes a strong line-broadening that renders these protons invisible in the static spectra. When the water content of the pore is increased, some of these protons are mobilized by exchange with water protons, as discussed above, which results in a more narrow line that is then visible in the static spectra too.

It is interesting to relate the stronger bound water found in SBA-15 to the model of the silica surface of SBA-15 (Figure 7) that was recently proposed by some of us.[23] The higher roughness of the silica surface is explained as incomplete silica layers on the inner surfaces. These incomplete layers might be the explanation for the observed stronger binding of some of the water molecules on the surface of SBA-15. On an ideal surface the −SiOH group distance is too large to permit a water molecule to form two hydrogen bonds to the surface at the same time. On the edges of a defect layer, however, it could be possible for a single water molecule to be involved simultaneously with two surface hydrogen bonds, thus nearly doubling its binding enthalpy.
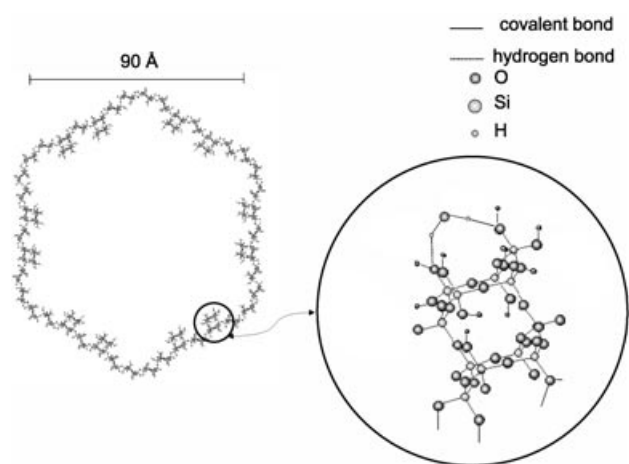
Figure 7. Left side: model of the surface of SBA-15 which shows possible surface defects (adapted from ref. [23]). Right side: enlargement of a surface defect with a sketch of a doubly hydrogen-bound water molecule, which is expected to have a higher binding enthalpy.

Conclusion

The adsorption of water in two different mesoporous silica materials with different pore diameters and internal surfaces, namely MCM-41 and SBA-15, was studied by employing ^{1}H MAS and static solid-state NMR spectroscopy. It is found that the filling cycle is completely reversible and that any adsorbed water can be removed by a vacuum pump, possibly accompanied by moderate heating with a heat gun. Various NMR lines of −OH hydrogen atoms are observed at different filling factors. The assignment of the line positions to individual types of −OH hydrogen atoms was done by merit of the chemical shift and corroborated by the line width of the static spectra. All observed hydrogen atoms are either surface −SiOH groups or hydrogen-bonded water molecules. No monomeric water molecules are observed at any filling level. It is found that in SBA-15 there exist some stronger bound water molecules on the surface that are only removable by the heat gun. These water molecules are tentatively assigned to surface defects that are present in SBA-15, but not in MCM-41. At higher filling levels an interesting difference between MCM-41 and SBA-15 is observed. In MCM-41 there is a bimodal-line distribution of chemical shifts of the water molecules, with one peak at the position of inner bulk water, and the second peak at the position of water molecules in fast exchange with surface −SiOH groups. In SBA-15 only a single line with a continuously varying chemical shift is observed. This result is an indication of different filling mechanisms for the two silica materials. In MCM-41, with its lower pore diameter, after an initial covering of the inner surfaces, the filling grows mainly in the direction of the pore axis. In SBA-15, however, owing to its larger pore diameter, the filling of the pore grows radially from the pore surface to the pore axis. This result has important consequences for the catalytic applications of these materials. Finally, it is shown that water can be employed to determine the surface density of −SiOH groups and is a sensor for surface inhomogeneity. From these results two new ques-

tions naturally arise, namely, are there H/D isotope effects on the filling mechanisms, and what is the temperature and pore-diameter dependence of the pore condensation in the silica pores? These questions are currently being studied in our laboratory.

[1] E. W. Hansen, M. Stöcker, R. Schmidt, *J. Phys. Chem.* **1996**, *100*, 2195.
[2] M. J. Setzer, *J. Colloid Interface Sci.* **2001**, *243*, 193.
[3] R. Kimmich, H. W. Weber, *Phys. Rev. B* **1993**, *47*, 788.
[4] R. Kimmich, F. Klammler, V. D. Skirda, I. A. Serebrennikova, A. I. Maklakhov, N. Fatkullin, *Appl. Magn. Reson.* **1993**, *4*, 425.
[5] R. Kimmich, *NMR Tomography Diffusometry Relaxometry*, Springer, Berlin, **1997**.
[6] J. Bodurka, A. Gutsze, G. Buntkowsky, H.-H. Limbach, *Z. Phys. Chem.* **1995**, *190*, 99.
[7] J. Bodurka, G. Buntkowsky, A. Gutsze, H.-H. Limbach, *Z. Naturforsch. C* **1996**, *51*, 81.
[8] J. Bodurka, G. Buntkowsky, R. Olechnowicz, A. Gutsze, H.-H. Limbach, *Colloids Surf. A* **1996**, *115*, 55.
[9] K. Overloop, L. Van Gerven, *J. Magn. Reson. Ser. A* **1993**, *101*, 179.
[10] Y. Hirama, T. Takahashi, M. Nino, T. Sato, *J. Colloid Interface Sci.* **1996**, *184*, 349.
[11] T. Ishizaki, M. Maruyama, Y. Furukawa, J. G. Dash, *J. Cryst. Growth* **1996**, *163*, 455.
[12] E. W. Hansen, E. Tangstad, E. Myrvold, T. Myrstad, *J. Phys. Chem. B* **1997**, *101*, 10709.
[13] K. Morishige, K. Nobuoka, *J. Chem. Phys.* **1997**, *107*, 6965.
[14] J. M. Baker, J. C. Dore, P. Behrens, *J. Phys. Chem. B* **1997**, *101*, 6226.
[15] T. Takamuku, M. Yamagami, H. Wakita, Y. Masuda, T. Yamaguchi, *J. Phys. Chem. B* **1997**, *101*, 5730.
[16] K. Morishige, K. Kawano, *J. Chem. Phys.* **1999**, *110*, 4867.
[17] C. Faivre, D. Bellet, G. Dolino, *Eur. Phys. J. B* **1999**, *7*, 19.
[18] J. Dore, *Chem. Phys.* **2000**, *258*, 327.
[19] K. Morishige, H. Iwasaki, *Langmuir* **2003**, *19*, 2808.
[20] J. S. Beck, J. C. Vartuli, W. J. Roth, M. E. Leonowicz, C. T. Kresge, K. D. Schmitt, C. T.-W. Chu, D. H. Olson, E. W. Sheppard, S. B. Mccullen, J. B. Higgins, J. L. Schlenker, *J. Am. Chem. Soc.* **1992**, *114*, 10834.
[21] D. Zhao, J. Feng, Q. Huo, N. Melosh, G. H. Fredrickson, B. F. Chmelka, G. D. Stucky, *Science* **1998**, *279*, 548.
[22] U. Ciesla, F. Schüth, *Microporous Mesoporous Mater.* **1999**, *27*, 131.
[23] I. Shenderovich, G. Buntkowsky, A. Schreiber, E. Gedat, S. Sharif, J. Albrecht, N. S. Golubev, G. H. Findenegg, H. H. Limbach, *J. Phys. Chem. B* **2003**, *107*, 11924.
[24] E. Gedat, A. Schreiber, G. Findenegg, I. Shenderovich, H.-H. Limbach, G. Buntkowsky, *Magn. Reson. Chem.* **2001**, *39*, 149.
[25] E. Gedat, A. Schreiber, J. Albrecht, I. Shenderovich, G. Findenegg, H.-H. Limbach, G. Buntkowsky, *J. Phys. Chem. B.* **2002**, *106*, 1977.
[26] R. Anwander, I. Nagl, M. Widenmayer, G. Engelhardt, O. Groeger, C. Palm, T. Röser, *J. Phys. Chem. B* **2000**, *104*, 3532.
[27] N. T. Whilton, B. Berton, L. Bronstein, H.-P. Hentze, M. Antonietti, *Adv. Mater.* **1999**, *11*, 1014.
[28] D. W. Aknes, L. Gjerdaker, *J. Mol. Struct.* **1999**, 27.
[29] F. Courivaud, E. W. Hansen, S. Kolboe, A. Karlsson, M. Stöcker, *Microporous Mesoporous Mater.* **2000**, *37*, 223.
[30] Y. B. Mel'nichenko, J. Schüller, R. Richert, B. Ewen, C.-K. Loong, *J. Chem. Phys.* **1995**, *103*, 2016.
[31] L. Gjerdaker, G. H. Sorland, D. W. Aknes, *Microporous Mesoporous Mater.* **1999**, *32*, 305.
[32] H. Jobic, *Phys. Chem. Chem. Phys.* **1999**, *1*, 525.

[33] V. Ladizhansky, G. Hodes, S. Vega, *J. Phys. Chem. B* **2000**, *104*, 1939.

[34] E. W. Hansen, R. Schmidt, M. Stöcker, D. Akporiaye, *Microporous Mater.* **1995**, *5*, 143.

[35] M. Grün, K. K. Unger, A. Matsumoto, K. Tsutsumi, *Charact. Porous Solids IV* **1997**, 81.

[36] A. Schreiber, I. Ketelsen, G. H. Findenegg, *Phys. Chem. Chem. Phys.* **2001**, *3*, 1185.

[37] D. Dollimore, G. R. Heal, *J. Appl. Chem.* **1964**, *14*, 109.